

Suspended InAs nanowire Josephson junctions assembled via dielectrophoresis

Domenico Montemurro^{1,2}, Daniela Stornaiuolo³, Davide Massarotti³, Daniele Ercolani¹, Lucia Sorba¹, Fabio Beltram¹, Francesco Tafuri², Stefano Roddaro¹

¹ NEST, Istituto Nanoscienze-CNR and Scuola Normale Superiore, Pisa I-56127, Italy

² Seconda Università degli Studi di Napoli, Dipartimento di Ingegneria dell'Informazione, Aversa (CE) I-81031, Italy

³ Università degli Studi di Napoli Federico II and CNR-SPIN, Napoli I Via Cinthia 26, I-80126, Italy

ABSTRACT

We present a novel technique for the realization of suspended Josephson junctions based on InAs semiconductor nanowires. The devices are assembled using a technique of drop-casting guided by dielectrophoresis that allows to finely align the nanostructures on top of the electrodes. The proposed architecture removes the interaction between the nanowire and the substrate which is known to influence disorder and the orientation of the Rashba vector. The relevance of this approach in view of the implementation of Josephson junctions based on High-Temperature Superconductors is discussed.

INTRODUCTION. Hybrid devices based on low-dimensional materials coupled to superconducting (SC) electrodes emerged in the last years as an ideal platform for the investigation unconventional quantum effects. In these devices the macroscopic quantum correlations typical of SCs can be induced via proximity effect in a wide class of low-dimensional materials such as graphene^{1,2} and semiconducting nanowires (NWs)³⁻⁷ that offer a unique degree of freedom in the design and control of quantum states⁸⁻¹¹. The most intriguing opportunity offered by these material combinations is the possibility to drive novel excitations and properties that none of the individual device components originally possessed. Recently, this possibility was at the base of the

proposal to obtain Majorana-like excitations in semiconducting NWs¹¹⁻¹⁵, where pairing correlations can be combined with Rashba spin-orbit coupling¹⁵⁻¹⁸. Hybrid NWs-SC Josephson junctions are typically obtained by transferring NWs to a Si/SiO₂ substrate, on top of which device electrodes are nanofabricated by aligned e-beam lithography. Future advancements in the field and a better understanding of the exotic excitations induced in NW-SC hybrid structures will also depend on the possibility to realize devices having complex architectures, such as systems comprising several NWs connected in a controlled way¹⁹. Moreover, in these hybrid devices the NW-to-substrate interaction is known to play an important role in terms of induced disorder and by the breaking of inversion symmetry in the electrostatic environment in which the nanostructure is embedded. This is believed to lead to a pinning of the Rashba vector within the plane of the host Si substrate²⁰. In this letter we demonstrate a rapid and effective method to realize NW-based suspended Josephson junctions where nanostructure positioning is obtained by dielectrophoresis (DEP) on previously patterned electrodes²¹⁻²³. In our devices, single NWs are aligned on electrode pairs separated by nanogaps approx. 100nm, corresponding to a dimension which is over one order of magnitude smaller than the NW length. This is an unusual and challenging DEP configuration and we discuss a novel geometry for achieving a good deposition in this regime. We also show that the properties of the hybrid devices realized using this method are comparable with those of conventional non-suspended devices. We believe that our DEP technique is suitable for the fabrication of a wide class of hybrid NW-based devices which can include, for instance, High critical Temperature Superconductors (HTS)²⁴. The relevance of our protocol for the implementation of field-effect HTS hybrid devices will be discussed.

DEVICE FABRICATION The structure of the suspended devices we realized is shown in Fig.1.

Junctions are fabricated using highly-doped n-type InAs NWs grown by chemical beam epitaxy²⁵ and characterized by a charge density of $n=1.8\pm 0.8 \times 10^{19} \text{cm}^{-3}$, a diameter of $90\pm 10 \text{nm}$ and an average length of $2\mu\text{m}$. The DEP electrodes are realized starting from a Ti/Au bilayer (10/100 nm) thermally evaporated on top of a SiO₂/Si substrate (280nm oxide) and patterned using a combination of UV and e-beam lithography. First, a set of bonding pads is defined by optical lithography, subsequently nanogaps are fabricated by e-beam lithography with a good reproducibility down to a gap size $d\approx 140 \text{nm}$ (Fig.1a). The design of the Ti/Au

electrodes is a crucial aspect of our method, since a suitable geometry is required to efficiently attract the NWs by DEP²⁶. Our optimal geometry is discussed in further details in the next Section. Following nanogap fabrication, NWs are placed across them using DEP-guided drop-casting (Fig.1b). In order to realize the SC contacts, a further e-beam lithographic step and thermal evaporation is used to define two $0.3 \times 1 \mu\text{m}^2$ Ti/Al (12/120nm) patches (Fig.1c) separated by a distance $L \propto d$, which will be regarded in the rest of the paper as the actual junction length. A good contact transparency between the metal and the NWs is ensured by a passivation step in an ammonium polysulfide (NH_4S_x) solution for 35 seconds at 44 °C prior to Ti/Al deposition. In parallel to the suspended junctions, conventional Al-NW weak links were fabricated also directly on top of the SiO_2/Si substrate in order to compare the properties of the devices in the two architectures. In this case the fabrication protocol was identical to the one used for the Ti/Al patches in the suspended devices.

GUIDING NANOWIRE DEPOSITION BY DIELECTROPHORESIS

DEP is a well-known technique for the controlled deposition of nano- and micro-scale structures. It exploits the forces exerted on a dielectric particle by the non-uniform electric field \mathbf{E} stemming from the induced dipole moment \mathbf{p} . In particular, when the size of the nano-/micro-structure can be neglected, one can expect a force and torque given by

$$\mathbf{F} = (\mathbf{p} \cdot \nabla) \mathbf{E} \quad (1)$$

$$\mathbf{T} = \mathbf{p} \times \mathbf{E} \quad (2)$$

The magnitude of the induced dipole \mathbf{p} depends on the complex dielectric functions of the DEP liquid medium $\varepsilon_m^*(\omega)$ and of the particle $\varepsilon_p^*(\omega)$, where $\omega = 2\pi\nu$ (ν is the frequency of the AC electric field and $\varepsilon^* = \varepsilon - j\sigma\omega$). The resulting force can be readily calculated for the case of a prolate ellipsoid: it is proportional to the gradient of the electrostatic energy following the law $\mathbf{F} \propto \varepsilon_m^*(\omega) \text{Re}[K_\alpha(\omega)] \nabla E^2$ where we introduced the Clausius-Massotti factors²¹

$$K_\alpha[(\omega)] = \frac{\varepsilon_p^* - \varepsilon_m^*}{A_\alpha(\varepsilon_p^* - \varepsilon_m^*) + \varepsilon_m^*}, \quad \alpha=L,S \quad (3)$$

The form factors A_α depend on the eccentricity e of the ellipsoid and attain two different values when the field is oriented along the long (L) or short (S) axes. Our NWs have a length which is ≈ 20 times the diameter; we can thus estimate $e = \sqrt{1 - (1/20)^2}$, leading²¹ to $A_L \approx 0.007$ and $A_S \approx 0.497$. The positive or negative sign of $\text{Re}[K_\alpha]$ determines whether the particle is attracted (positive DEP) or repelled (negative DEP) from regions with large \mathbf{E} . Since our DEP protocol was performed using isopropyl alcohol ($\varepsilon_m \approx 18$ and negligible conductivity $\sigma_m \approx 6\mu\text{S}/\text{m}$) as the medium and highly-doped InAs NWs as the "particle" ($\varepsilon_p \approx 10$ and sizable conductivity $\sigma_p \approx 10^5\text{S}/\text{m}$), deposition is expected to work already at rather low frequencies²⁷. Provided the correct DEP sign is achieved, the force in equation (1) will tend to attract the nanostructure to regions with a large electric field, the torque in equation (2) will tend to align the NWs to the field lines thanks to their easier polarizability along the axis. Usually, DEP is performed using electrodes separated by a gap of size comparable to that of the target nanostructures. In our case, on the other hand, we need to position the NWs on top of electrodes separated by a gap with a size d approx. 100-200nm, thus 10-20 times smaller than the NW length; this is an unusual configuration for DEP. One issues with such a small-gap geometry is that the field \mathbf{E} in the gap can become very strong even for relatively moderate excitation voltages, with a significant risk of destructive electrostatic discharges. This poses strict limitations to the highest voltage that can be safely applied to the electrodes and, in turn, reduces the size of the region where DEP forces are able to overcome the effect of Brownian motion and random liquid convection and thus to actually capture NWs. In addition, for small structures, trapping forces converging to the gap occur in a region which can easily be even smaller than the

NW size and rapidly decay in the surrounding volume; therefore they are not very effective in trapping the nanostructure. These issues motivated us to develop a new DEP electrode geometry. In order to obtain a four-wire contact geometry, we designed two facing electrodes with a "U" shape and large surface coverage so that a sizable E field could be induced over a significant volume and lead to a larger capture cross-section. Prior to the fabrication, we performed numerical simulations of the induced DEP field for structures of various dimensions. In Fig.2 we compare predictions²⁸ for a standard case of two 1 μ m-wide fingers separated by a thin gap of 200nm (panel a) and for a w=10 μ m gap geometry (panel b), which reproduce the experimental configuration of Fig.1e. In both cases we plot the modulus of the gradient of the electrostatic energy density for a biasing voltage of ± 1 V at the two electrodes and using $\epsilon_m=18.23$ for the isopropyl alcohol. A 2 μ m-long NW was added as a length reference. The comparison indicates that the second geometry is more effective in capturing the DEP is a well-known technique for the controlled deposition of nano- and micro-scale structures. It exploits the forces exerted on a dielectric particle by the non-uniform electric field \mathbf{E} stemming from the induced dipole moment \mathbf{p} . In particular, when the size of the nano-/micro-structure can be neglected, one can expect a force and torque given by

$$\mathbf{F} = (\mathbf{p} \cdot \nabla) \mathbf{E} \quad (1)$$

$$\mathbf{T} = \mathbf{p} \times \mathbf{E} \quad (2)$$

The magnitude of the induced dipole \mathbf{p} depends on the complex dielectric functions of the DEP liquid medium $\epsilon_m^*(\omega)$ and of the particle $\epsilon_p^*(\omega)$, where $\omega = 2\pi\nu$ (ν is the frequency of the AC electric field and $\epsilon^* = \epsilon - j\sigma\omega$). The resulting force can be readily calculated for the case of a prolate ellipsoid: it is proportional to the gradient of the electrostatic energy following the law $\mathbf{F} \propto \epsilon_m^*(\omega) \text{Re}[K_\alpha(\omega)] \nabla E^2$ where we introduced the Clausius-Massotti factors²¹

$$K_\alpha[(\omega)] = \frac{\epsilon_p^* - \epsilon_m^*}{A_\alpha(\epsilon_p^* - \epsilon_m^*) + \epsilon_m^*}, \quad \alpha=L,S \quad (3)$$

The form factors A_α depend on the eccentricity e of the ellipsoid and attain two different values when the field is oriented along the long (L) or short (S) axes. Our NWs have a length which is ≈ 20 times the diameter; we can thus estimate $e = \sqrt{1 - (1/20)^2}$, leading²¹ to $A_L \approx 0.007$ and $A_S \approx 0.497$. The positive or negative sign of $\text{Re}[K_\alpha]$ determines whether the particle is attracted (positive DEP) or repelled (negative DEP) from regions with large \mathbf{E} . Since our DEP protocol was performed using isopropyl alcohol ($\epsilon_m \approx 18$ and negligible conductivity $\sigma_m \approx 6\mu S/m$) as the medium and highly-doped InAs NWs as the "particle" ($\epsilon_p \approx 10$ and sizable conductivity $\sigma_p \approx 10^5 S/m$), deposition is expected to work already at rather low frequencies²⁷. Provided the correct DEP sign is achieved, the force in equation (1) will tend to attract the nanostructure to regions with a large electric field, the torque in equation (2) will tend to align the NWs to the field lines thanks to their easier polarizability along the axis. Usually, DEP is performed using electrodes separated by a gap of size comparable to that of the target nanostructures. In our case, on the other hand, we need to position the NWs on top of electrodes separated by a gap with a size d approx. 100-200nm, thus 10-20 times smaller than the NW length; this is an unusual configuration for DEP. One issues with such a small-gap geometry is that the field \mathbf{E} in the gap can become very strong even for relatively moderate excitation voltages, with a significant risk of destructive electrostatic discharges. This poses strict limitations to the highest voltage that can be safely applied to the electrodes and, in turn, reduces the size of the region where DEP forces are able to overcome the effect of Brownian motion and random liquid convection and thus to actually capture NWs. In addition, for small structures, trapping forces converging to the gap occur in a region which can easily be even smaller than the NW size and rapidly decay in the surrounding volume; therefore they are not very effective in trapping the nanostructure. These issues motivated us to develop a new DEP electrode geometry. In order to obtain a four-wire contact geometry, we designed two facing electrodes with a "U" shape and large surface coverage so that a sizable E field could be induced over a significant volume and lead to a larger capture cross-section.

Prior to the fabrication, we performed numerical simulations of the induced DEP field for structures of various dimensions. In Fig.2 we compare predictions²⁸ for a standard case of two 1 μm -wide fingers separated by a thin gap of 200nm (panel a) and for a $w=10\mu\text{m}$ gap geometry (panel b), which reproduce the experimental configuration of Fig.1e. In both cases we plot the modulus of the gradient of the electrostatic energy density for a biasing voltage of $\pm 1\text{V}$ at the two electrodes and using $\epsilon_m=18.23$ for the isopropyl alcohol. A 2 μm -long NW was added as a length reference. The comparison indicates that the second geometry is more effective in capturing the NWs and orienting them along the planned direction, for a given electrode bias since DEP forces extend further away from the gap with respect to the case of panel (a). This is even more evident looking at the white lines on the right-hand side plots, which indicate the direction of the DEP action: in our DEP geometry attractive forces converge to the gap over a rather large volume; differently, as anticipated, a much poorer capture efficiency can be expected in the more standard geometry of panel (a). Experimentally, our DEP process was achieved as follows. InAs NWs were dispersed in isopropanol by sonication of the growth substrate. The deposition was then achieved by putting a drop (2 μl) of the solution on the substrate and, at the same time, by applying an AC voltage to the Ti/Au electrodes, as indicated in the overlay in Fig.1d. Since we use a very small inter-electrode gap, the substrate is largely screened. As a consequence, it is not expected to have an important effect and can be left floating²¹. Optimal results were obtained by applying an AC voltage in the range 0.75 - 1.20V and a frequency of 1-10kHz, while frequencies $\nu \leq 10\text{Hz}$ were found to be less effective²¹⁻²³. The AC field was applied until the isopropanol completely dried up. These values gave a good deposition yield, without accumulation of NW clusters. A typical device obtained using this process is shown in Fig.1e.

ELETRICAL TRANSPORT MEASUREMENTS

Devices fabricated following the DEP protocol described in the previous section yielded Josephson junctions with properties which were found to be comparable to those typically observed in the more standard non-suspended architecture. The transport properties of the devices were measured from room temperature down to 300mK using a Heliox refrigerator. The measurement system was magnetically shielded, using superconducting screens, and the lines were filtered using RC filters and two stages of copper-powder filters. Figure 3 shows typical Resistance vs. Temperature ($R(T)$) curves of suspended devices fabricated starting from nano-trenches of different sizes d (see Fig.1e) and having a channel length $L \approx d$. Since the room-temperature normal resistance R_N of the devices ranges from 180 to 400 Ω , the plot shows the resistances normalized to their values at $T=1.4\text{K}$. The curves were recorded using a lock-in technique with an excitation current of 5nA. From room temperature down to $T=1.1\text{K}$ the $R(T)$ curves show a similar insulating trend (data not shown) independently from the extension L of the normal region. For all devices, a drop in the resistance is observed at $T=1.1\text{K}$, as a consequence of the superconducting transition of the Ti/Al pads. Below this temperature, we observed a different behavior depending on the L parameter. For devices with $L \leq 150\text{nm}$, a complete superconducting transition was typically recorded. These results clearly indicate the influence of the channel length L on the proximity effect across the contact barriers and into the NWs.

The current vs. voltage (I - V) characteristics of the superconductive devices were carefully analyzed as a function of temperature: selected curves are shown in Fig.4a for device D7B. The behavior of this devices is typical of that of an overdamped Josephson junction showing phase-diffusion effects that become particularly evident for $T > 400\text{mK}$ ^{29,30}. The critical current, extracted using a $V = 1\mu\text{V}$ threshold, is $I_c = 62\text{nA}$ at $T = 300\text{mK}$; this value corresponds to a critical-current density of about 1.0kA/cm², in agreement with the values typically found for this type of InAs NWs⁷. These superconducting properties are comparable to those of conventional devices fabricated directly on the Si/SiO₂ substrate. The I - V characteristic of one of these conventional devices (D7T) is reported in Fig.4b and exhibits an I_c value at 300mK similar to the one obtained in suspended device D7B. This comparison confirms that the discussed DEP method provides a valid route for the realization of high quality hybrid devices on narrow-gap electrodes. Starting from the normal transport properties of the InAs NWs, we estimate a diffusion coefficient $D = 0.02\text{m}^2/\text{s}$, a Thouless Energy $E_{Th} = \hbar D/L^2$ and a normal coherence length $\xi_N = \sqrt{\hbar D/(2\pi k_B T)} = 300\text{nm}$; these parameters indicate that the devices operate in the diffusive short-junction limit. Further insight in the transport mechanisms of the suspended devices can be obtained from the temperature dependence of the Josephson critical current

$I_c(T)$, which we show in Fig.4c. We compare the experimental I_c vs. T behavior with a model which takes into account the barrier transparency. The upper concavity of the I_c vs T curve of Fig.4c is indeed an indication of a sizable superconducting (S)-normal (N) interface resistance, as shown in Ref.31}. In this framework, the energy scale ruling the $I_c(T)$ dependence is an effective Thouless Energy E_{Th}^* which takes into account the ratio between the resistances of the S/N interfaces and the one of the normal conductor. Our experimental data can be well approximated by an exponential function³²:

$$I_c \propto \exp(-T/T^*) \quad (4)$$

where T^* is linked to the reduced Thouless energy by $E_{Th}^*=2\pi k_B T^*/24$. The fit is shown as a solid red line in Fig.4c and was obtained with a value $E_{Th}^*=3.1\mu\text{eV}$, confirming the effect of the interface resistance in hampering the superconducting proximization of the NW. Finally, in Fig.5 we show the temperature evolution of the differential resistance dV/dI curves as a function of the voltage in the sub-gap region (considering $\Delta=120\mu\text{eV}$ for Al), as visible in Fig.5. Symmetric structures are observed at $V\approx 10$ and $25\mu\text{eV}$. The voltage position of these peaks is not influenced by temperature and suggests they cannot be linked to multiple Andreev reflections. However, the amplitude of the peaks decreases as the temperature is increased and is almost completely suppressed at $T=720\text{mK}$: this evolution indicates that these structures do have some connection with superconductivity. Several works in the literature reported the appearance of differential resistance peaks having similar temperature behavior and related them to the coupling of Josephson oscillations to the acoustic degrees of freedom of the suspended NWs³³ However, since we observed similar peaks also in non-suspended devices (inset of Fig.5), we believe this interpretation is not applicable to our case. S. Abay and coworkers in Ref.34 suggested an alternative mechanism based on the presence of inhomogeneities in the NW. In this scenario, the observed peaks would be related to the sequential appearance of normal domains in the NW as the current is increased. The presence of an inhomogeneous resistive state in the NW region in proximity with Al is supported in our case by the peculiar shape of the $R(T)$ curves. As visible from the data of Fig.3, the $R(T)$ curve of devices with L in the range 150 - 160nm exhibit a large plateau which extends from the superconductive onset of the Al patches at $T=1.1\text{K}$, down to $T=500\text{mK}$.

CONCLUSIONS In conclusion, we have demonstrated a novel DEP technique for the fabrication of suspended Josephson junctions. Since the inter-electrode gap in our device architecture is much smaller than the NW dimension, a novel DEP geometry was simulated and experimentally tested. The possibility to decouple the NW from the SiO_2 substrate is a desirable feature since it is expected to lead to a reduced scattering and to avoid the symmetry breaking effects stemming from NW-substrate interactions. The comparison between suspended and non-suspended devices indicates that the fabrication protocol is robust. We note that in our protocol the superconductive electrodes can be fabricated before NW deposition. This is a crucial difference which can enable to use of superconductors whose growth/deposition conditions are not compatible with the chemical and structural stability of the NWs. In particular it could be combined with HTS layers which require rather extreme growth conditions. The fabrication of HTS-NW Josephson junctions could be relevant to the observation of Majorana excitations in hybrid systems²⁴, allow higher operation temperatures and a more robust behavior in external magnetic fields.

Acknowledgements

This work was supported by the Italian MIUR FIRB project *HybridNanoDev RBFR1236VV001* and by *POR Campania FSE 2007-2013 "MATERiali e STRutture Intelligenti" MASTRI*.

References

- [1] Hubert, B.H. and Jarillo-Herrero, P- and Oostinga, J.B. and Vandersypen, L.M.K. and Morpurgo A.F. Bipolar supercurrent in graphene, *Nature*, 2007, 446, 56-59

- [2] Mizuno, N. and Nielsen, B. and Du, X. Ballistic-like supercurrent in suspended graphene Josephson weak links Nature Communication, 2013, 4, 2716
- [3] De Franceschi, S. and Kouwenhoven, L. and Schonenberg, C. and Wernsdorfer, W. Hybrid superconductor-quantum dot devices. Nature Nanotechnology, 2010, 5, 703-711
- [4] Doh, Y.-J. and van Dam, J.A. and Roest, A.L. and Bakkers, E.P.A.M. and Kouwenhoven, L.P. and De Franceschi, S. Tunable Supercurrent Through Semiconductor Nanowires, Science, 2005, 309, 272
- [5] Giazotto, F. and Panayotis, S. and Roddaro, S. and Biswas, S. and Taddei, F. and Governale, M. and Sorba, L. A Josephson quantum electron pump, Nature Physics, 2011, 7, 857-861
- [6] Spathis, P. and Biswas, S. and Roddaro, S. and Sorba, L. and Giazotto, F. and Beltram, F. Hybrid InAs nanowire-vanadium proximity SQUID, Nanotechnology, 2011, 22, 105201
- [7] Roddaro, S. and Pescaglioni, A. and Ercolani, D. and Sorba, L. and Giazotto, F. and Beltram F. Hot-Electron Effects in InAs Nanowire Josephson Junctions, Nano Research, 2011, 4, 259
- [8] Romeo, L. and Roddaro, S. and Pitanti, A. and Ercolani, D. and Sorba, L. and Beltram, F. Electrostatic Spin Control in InAs/InP Nanowire Quantum Dots, Nano Letters, 2012, 12, 4490-4494
- [9] Rossella, F. and Bertoni, A. and Ercolani, D. and Rontani, M. and Sorba, L. and Beltram, F. and Roddaro, Nanoscale spin rectifiers controlled by the Stark effect, Nature Nanotechnology, 2014, 9, 997-1001
- [10] Ganjipour, B. and Sepehri, S. and Dey, A.W. and Tizno, O. and Borg, B.M. and Dick, K.A. and Samuelson, L. and Wernersson, L.-E. and Thelander, C. Electrical properties of GaSb/InAsSb core/shell nanowires, Nanotechnology, 2014, 25, 425201
- [11] Lee, E.J.H. and Jiang, H. and Houzet, M. and Aguado, R. and Lieber, C.M. and De Franceschi, S. Spin-resolved Andreev levels and parity crossings in hybrid superconductor-semiconductor nanostructures, Nature Nanotechnology, 2014, 9, 79-84
- [12] Rokhinson, Leonid P and Liu, Xinyu and Furdyna, Jacek K. The fractional ac Josephson effect in a semiconductor-superconductor nanowire as a signature of Majorana particles, Nature Physics, 2012, 8,11, 795-799
- [13] Das, Anindya and Ronen, Yuval and Most, Yonatan and Oreg, Yuval and Heiblum, Moty and Shtrikman, Hadas. Zero-bias peaks and splitting in an Al-InAs nanowire topological superconductor as a signature of Majorana fermions, Nature Physics, 2012, 8,12, 887--895
- [15] Mourik, Vincent and Zuo, Kun and Frolov, SM and Plissard, SR and Bakkers, EPAM and Kouwenhoven, LP. Signatures of Majorana fermions in hybrid superconductor-semiconductor nanowire devices, Science, 2012, 336, 6084, 1003-1007
- [16] Alicea, Jason. Exotic matter: Majorana modes materialize, Nature Nanotechnology, 2013, 8,9, 623-624
- [17] Lutchyn, Roman M and Sau, Jay D and Sarma, S Das. Majorana fermions and a topological phase transition in semiconductor-superconductor heterostructures, Phys. Rev. Lett., 2010, 105, 7, 077001
- [18] Oreg, Yuval and Refael, Gil and von Oppen, Felix Helical liquids and Majorana bound states in quantum wires, Phys. Rev. Lett., 2010, 105, 17, 177002
- [19] Altland, Alexander and Egger, Reinhold Multiterminal Coulomb-Majorana Junction, Phys. Rev. Lett., 2013, 110, 19, 196401
- [20] Nadj-Perge, S. and Pribiag, V.S. and van den Berg, J.W.G. and Zuo, Z. and Plissard, S.R. and Bakkers, E.P.A.M. and Frolov, S.M. and Kouwenhoven, L.P. Spectroscopy of Spin-Orbit Quantum Bits in Indium Antimonide Nanowires, Phys. Rev. Lett., 2012, 108, 166801
- [21] Maijenburg, A.W. and Maas, M.G. and Rodijk, E.J.B. and Ahmed, W. and Kooij, E.S. and Carlen, E.T. and Blank, D.H.A. and Elshof, J.E. Dielectrophoretic alignment of metal and metal oxide nanowires and nanotubes: A universal set of parameters for bridging prepatterned microelectrodes, Jour. of Colloid and Interface Science, 2011, 355, 486-493
- [22] Smith, Peter A. and Nordquist, Christopher D. and Jackson, Thomas N. and Mayer, Theresa S. and Martin, Benjamin R. and Mbindyo, Jeremiah and Mallouk, Thomas E. Electric-field assisted assembly and alignment of metallic nanowires, Appl. Phys. Lett., 2000, 771399
- [23] Hesketh, P.J. and Gallivan, M.A. and Kumar, S. and Erdy, C.J. and Wang Z.L. The application of dielectrophoresis to nanowire sorting and assembly for sensors, Proceeding of the 13th Mediterranean Conference on Control and Automation, 2005
- [24] Lucignano, P. and Mezzacapo, A. and Tafuri, F. and Tagliacozzo, A. Advantages of using high-temperature cuprate superconductor heterostructures in the search for Majorana fermions, Phys. Rev. B, 2012,86, 144513
- [25] Panda, J.K. and Roy, A. and Singha, A. and Gemmi, M. and Ercolani, D. and Pellegrini, V. and Sorba, LRaman sensitivity to crystal structure in InAs nanowires, Appl. Phys. Lett., 2012, 100, 14310
- [26] Xu, D. and Subramanian, A. and Dong, L. and Nelson, J.B. Shaping Nanoelectrodes for High-precision Dielectrophoretic Assembly of Carbon Nanotubes, IEEE Trans. on Nanotech., 2009, 8, 449
- [27] Very low frequencies ($\nu \ll 1KHz$), though, should still be avoided since DEP is expected to be less effective in this regime²¹⁻²³
- [28] Calculations were performed with the PDE solver avoided COMSOL Multiphysics 3.5a.
- [29] A. Barone, G. Paterno, Physics and applications of the Josephson effect, Wiley 1982
- [30] Stornaiuolo, D and Rotoli, G and Massarotti, D and Carillo, F and Longobardi, L and Beltram, F and Tafuri, F Resolving the effects of frequency-dependent damping and quantum phase diffusion in $YBa_2Cu_3O_{7-x}$ Josephson junctions, Physical Review B, 2013, 87,13, 134517
- [31] Hammer, JC and Cuevas, Juan Carlos and Bergeret, FS and Belzig, Wolfgang Density of states and supercurrent in diffusive SNS junctions: Roles of nonideal interfaces and spin-flip scattering, Physical Review B, 2007, 76, 6, 064514
- [32] Carillo, Franco and Born, Detlef and Pellegrini, Vittorio and Tafuri, Francesco and Biasiol, Giorgio and Sorba, Lucia and

Beltram, Fabio Relevant energy scale in hybrid mesoscopic Josephson junctions, Physical Review B, 2008, 78, 5, 052506

[33] Kretinin, Andrey and Das, Anindya and Shtrikman, Hadas The self-actuating InAs nanowire-based nanoelectromechanical Josephson junction, arXiv preprint arXiv:1303.1410, 2013

[34] Abay, Simon and Persson, Daniel and Nilsson, Henrik and Wu, Fan and Xu, H. Q. and Fogelstrom, Mikael and Shumeiko, Vitaly and Delsing, Per Charge transport in InAs nanowire Josephson junctions, Phys. Rev. B, 2014, 89

Figures

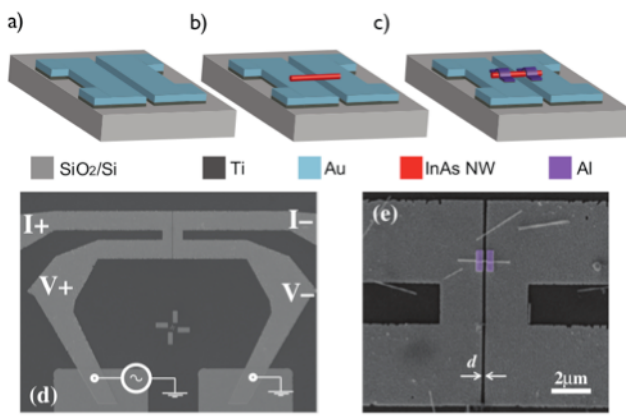


Figure 1 A sketch of the fabrication procedure is visible in the top panels: Ti/Au electrodes (blue) with a nanotrench are fabricated by a combination of e-beam and optical lithography (a), InAs nanowires (red) are deposited across the inter-electrode gap by a dielectrophoresis technique (b) and contacted with two $0.3 \times 1 \mu\text{m}^2$ superconductive Ti/Al patches (violet) (c). Panel (d) shows the layout of the Ti/Au contact geometry, the overlay indicates the AC bias system used to achieve a deposition guided by dielectrophoresis. Panel (e) shows an example of a complete device, with the Ti/Al patches in violet.

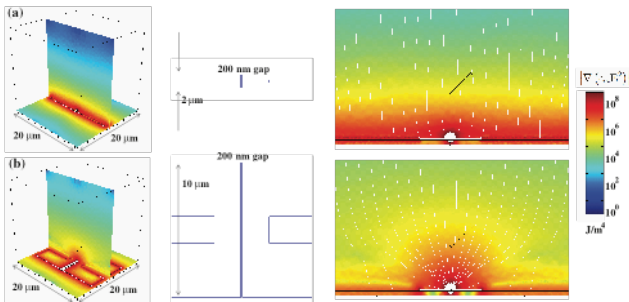


Figure 2 Numerical simulations for the gradient of the electrostatic energy density $|\nabla \epsilon \mathbf{E}^2 / 2|$ for two different electrode configurations. Panel (a) refers to double finger architecture with a lateral size of $1 \mu\text{m}$ and a gap of 200 nm . Panel (b) refers to the geometry shown in Fig.1. In both cases a $\pm 1 \text{ V}$ bias was applied to the two electrodes and using $\epsilon_m = 18.23$ for the isopropyl alcohol. On the right hand side white lines indicate the direction of the gradient and highlight the more efficient trapping of the geometry in panel (b). It is important to note that the field line density in the right panels does not have any direct correspondence with $|\mathbf{E}|$ since the field configuration is three-dimensional and has a strong dependence on the out-of-plane direction, particularly in thin-finger the case (a). A $2 \mu\text{m}$ long cylinder was added as a reference at about $3 \mu\text{m}$ from the electrodes.

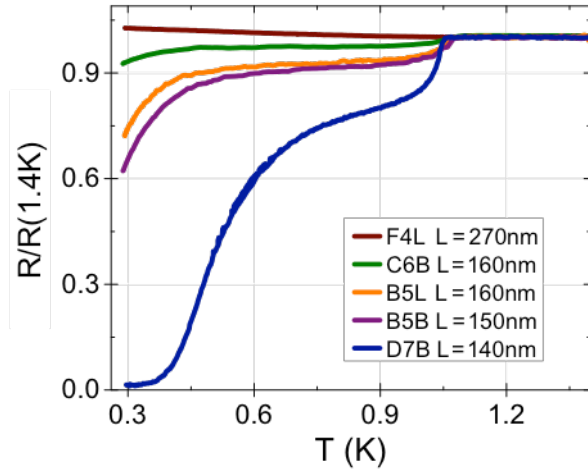


Figure 3 Normalized $R(T)/R(1.4K)$ curves of suspended devices characterized by a different channel length L . A different behavior is observed as a function of L : devices with $L < 200nm$ display a metallic behavior instead if $L < 150nm$ a full transition to the superconductive regime is obtained.

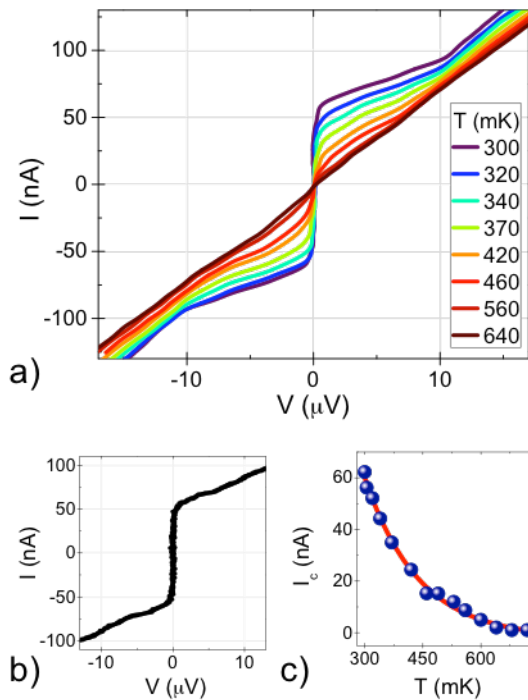


Figure 4 I-V characteristics of suspended device D7B as a function of temperature (a) and of conventional non-suspended device D7T at $T=300mK$ (b). The two devices have the channel length $L=140nm$. The I_c vs T of device D7B (blue dots) is visible in panel (c). The full red line is the fit obtained using equation 4.

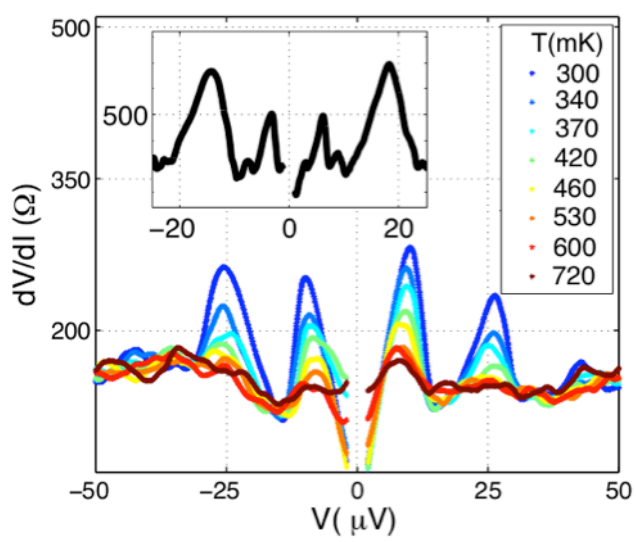


Figure 5 Differential resistance dV/dI as a function of V of suspended device D7B for selected temperatures. The low voltage part of the data (where superconductivity is present) was cut for clarity. Only the sub-gap region is shown in order to highlight the presence of peaks with temperature independent voltage position. Similar peaks are visible also in the dV/dI curve of non-suspended device D7T, which is shown in the inset.